AGU100 ADVANCING EARTH AND SPACE SCIENCE

Geophysical Research Letters

RESEARCH LETTER
10.1029/2019GL083503

Aerosol-Mediated Glaciation of Mixed-Phase Clouds: Steady-State Laboratory Measurements

N. Desai[1], K. K. Chandrakar[1], G. Kinney[1], W. Cantrell[1], and R. A. Shaw[1]

[1]Atmospheric Sciences Program, Department of Physics, Michigan Technological University, Houghton, MI, USA

Abstract What concentration of ice-nucleating particles is required to completely glaciate a typical atmospheric supercooled liquid cloud? This seemingly esoteric question has far reaching implications, as the ratio of liquid to ice in these clouds governs, for example, their influence on Earth's radiation budget and their precipitation efficiency. Microphysical properties of steady-state mixed-phase clouds formed in a laboratory convection chamber are observed using digital holography. It is observed that the ratio of ice to total water content of steady-state mixed-phase clouds is determined by the concentration of ice-nucleating aerosol particles. Existing theory is adapted to show such clouds result from a balance between the thermodynamic forcing (i.e., the source of excess water vapor that is condensing to liquid and ice) and the number and size of particles that become ice (i.e., the ice integral radius). The measurements quantitatively support the Korolev-Mazin conditions for existence of mixed-phase clouds.

Key Points:
- Holographic measurements of steady-state mixed-phase clouds are made in a laboratory cloud-convection chamber
- The ice fraction in the cloud is determined by varying the ice-nucleating particle concentration while holding CCN concentration constant
- Measurements are in agreement with an extension of Korolev-Mazin theory for critical forcing needed for mixed-phase conditions

Supporting Information:
- Supporting Information S1

Correspondence to:
R. A. Shaw and W. Cantrell,
rashaw@mtu.edu;
cantrell@mtu.edu

Citation:
Desai, N., Chandrakar, K. K., Kinney, G., Cantrell, W., & Shaw, R. A. (2019). Aerosol-mediated glaciation of mixed-phase clouds: Steady-state laboratory measurements. *Geophysical Research Letters*, *46*, 9154–9162. https://doi.org/10.1029/2019GL083503

Received 27 APR 2019
Accepted 10 JUL 2019
Accepted article online 18 JUL 2019
Published online 2 AUG 2019

1. Introduction

At temperatures below 0 °C, clouds in Earth's atmosphere are observed to exist and persist in a thermodynamically unstable state for hours to days (Morrison et al., 2012; Shupe et al., 2006; Westbrook & Illingworth, 2013). Such clouds are called "mixed phase" because of the coexistence of liquid water and ice hydrometeors. Mixed-phase clouds play critical roles in precipitation over the continents (Field & Heymsfield, 2015; Mülmenstädt et al., 2015) and are implicated in summer-time sea-ice loss in the Arctic (Kay & Gettelman, 2009) and strong radiative signatures over the Southern Ocean (Vergara-Temprado et al., 2018). The properties of mixed-phase clouds are fundamentally different from either liquid water or ice clouds of the same condensed water mass (Korolev et al., 2017). Understanding the mechanisms responsible for maintenance or dissipation of mixed-phase clouds is therefore of the utmost importance.

Numerous field campaigns and numerical simulations (Curry et al., 1997; Fridlind et al., 2012; Hill et al., 2014; Korolev & Isaac, 2003; McFarquhar & Cober, 2004; Pinsky et al., 2018; Pinto, 1998; Verlinde et al., 2007; Zawadzki et al., 2000) have been devoted to investigating the microphysical properties of mixed-phase clouds. They can persist for days or rapidly glaciate within a few minutes (e.g., Lawson et al., 2015; Kalesse et al., 2016; Pinsky et al., 2018; Shupe et al., 2011). This variability in cloud lifetime significantly affects their radiative properties and relevance (Garrett & Zhao, 2006; Sun & Shine, 1995); it also makes mixed-phase clouds challenging to represent in climate models (Furtado et al., 2016; Storelvmo et al., 2008). To further complicate matters, it is observed that mixed-phase clouds can be sensitive to aerosol properties (Fan et al., 2017; Fu & Xue, 2017; Norgren et al., 2018; Prenni et al., 2007); the resulting indirect effects are another important source of uncertainty in representing clouds in large-scale models (Lohmann, 2002).

We approach mixed-phase clouds from the perspective of a well-controlled laboratory experiment where the conflating influences of large-scale dynamics and poorly defined boundary conditions, which complicate the interpretation of both field measurements and simulations, can be minimized or eliminated. Our focus is the effect of aerosol on the partitioning between liquid water and ice for a constant thermodynamic forcing. The traditional view of phase partitioning, dating back to Alfred Wegener and described more completely by the Wegener-Bergeron-Findeisen (WBF) process (Lamb & Verlinde, 2011, chapter 12), is that ice crystals may grow at the expense of surrounding liquid water droplets. This is so because, for the same temperature, the equilibrium vapor pressure over ice is less than the equilibrium vapor pressure over liquid water. While that view is true in a static environment, the environmental vapor pressure in a cloud is continually changing, and more recent work has shown that phase partitioning is governed by inequalities among the environmental vapor pressure, the equilibrium vapor pressure over the liquid, and the equilibrium vapor

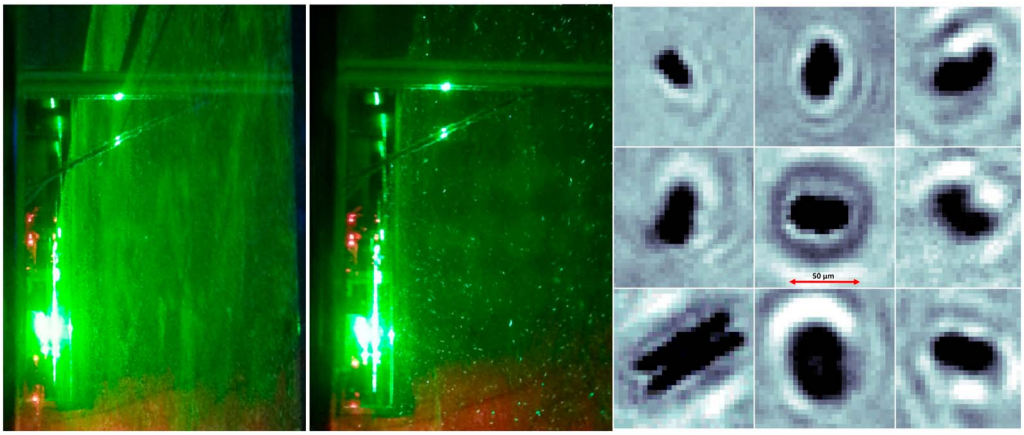

Figure 1. (left) Supercooled liquid cloud produced by injecting NaCl aerosols into the chamber with mean temperature $T_m = -6.7$ °C. (center) Mixed-phase cloud generated after introduction of Snomax aerosols to the previously generated liquid cloud. We can see that the mixed-phase cloud has lower droplet number concentration and visually apparent sparkles from ice crystals. (right) Some ice particles as seen in the holograms. The size and the shape of these particles is not the same as ice crystals found in atmospheric measurements due to the small particle lifetimes inside the laboratory chamber.

pressure over ice (Korolev, 2007). Depending upon the strength of the updraft in the cloud, liquid water may evaporate and ice grow (as in the WBF process), both liquid water and ice may grow, or both may evaporate. Hill et al. (2014) showed through a turbulent large eddy simulation (LES) model that ice number concentration plays an important role as well and is negatively correlated with liquid water content. In this paper, we investigate the complementary questions, "What are the conditions for existence of mixed-phase clouds in steady state in spite of being in a thermodynamically unstable state?" and "How do the microphysical properties of those mixed-phase clouds respond to varying concentrations of ice-nucleating particles (INPs) relative to concentrations of cloud condensation nuclei (CCN)?"

The paper proceeds as follows: In section 2, we explain the experimental setup used to generate steady-state, mixed-phase clouds. In section 3, we extend theoretical predictions of phase partitioning to the case of constant forcing but varying input of INPs, and then in section 4, we present the results of the experiments and, where possible, compare to the predictions developed in section 3. Finally, in section 5, we summarize the main results and discuss implications for the atmospheric context.

2. Experimental Approach

2.1. Chamber setup

To generate a steady-state, mixed-phase cloud, we use turbulent mixing in the Michigan Tech Π-Chamber. The facility is described in more detail in Chang et al. (2016). We outline the important aspects of our experiments here. The bottom surface of the chamber is maintained at $T_b = 4$ °C and saturated with liquid water. The top surface is maintained at $T_t = -16$ °C. This surface is also covered with water but is frozen, so the vapor pressure at the top boundary is ice saturation. The temperature gradient between these boundaries creates turbulent convection, and the associated isobaric mixing of air parcels originating from the bottom and top saturated surfaces leads to a supersaturated environment. While the turbulent mixing creates the conditions for cloud formation, to actually create a cloud, we inject NaCl particles (20,000 cm^{-3} at 2 lpm into the chamber), which act as CCN. An example of the resulting, supercooled cloud is shown in the left panel of Figure 1. The cloud is in steady state when the rate of activation of CCN (i.e., formation of cloud droplets) balances the removal of droplets by gravitational settling. In steady state, the measured time series of cloud droplet number and size are stationary. For this injection rate of CCN, a liquid water cloud with droplets with a mean diameter of 15.5 μm and a number concentration of 25 cm^{-3} is generated in the chamber.

After achieving a steady-state, supercooled liquid cloud, INPs (Snomax) are injected into the chamber to catalyze ice formation. The details of the nucleation process are not the emphasis here, only the response of the cloud to the newly formed ice particles. Snomax is dispersed using a shaking flask, at a steady rate at 4 lpm of inlet air flow. It is commercially available and is known to nucleate ice at temperatures as high as approximately −4 °C (Wex et al., 2015) which is close to the mean temperature in this study. Clouds were

allowed to relax to steady state for a range of Snomax injection rates, from 0.15 to 5.00 cm^{-3} min^{-1} in the inlet flow. (Since Snomax is the only INP used in this experiment, we will refer to it as INP from here on.) An example of a mixed-phase cloud is shown in the center panel of Figure 1. The optical depth has decreased, and bright glints, which are ice crystals, are apparent in the image.

2.2. Holographic Setup

For quantitative detection of ice, we use digital in-line holography. The holographic setup used for the measurements is the same as described in Desai et al. (2018). A burst of nine consecutive images recorded at 500 frames per second were taken every 30 s for 2.5 hr. The image groups were used to eliminate background noise by averaging to produce a single data point every 30 s. Those digital holograms were then numerically reconstructed at every 100 μm position along the laser beam axis over 20 cm of the measurement volume using the convolution method in Fourier space (Fugal et al., 2004). This gives each hologram a measurement volume of 10 cm^3. The reconstructed images are then analyzed to find particles and their equivalent diameters using a light intensity threshold (Lu et al., 2008). The minimum resolution is 7 μm in diameter, and for the given experimental conditions, the primary modes of cloud droplets and ice are above this threshold. Examples of ice crystals detected in the experiments are shown in the right panel of Figure 1.

3. Theory

As noted above, a mixed-phase cloud containing all three phases of water is thermodynamically unstable due to the difference in saturation vapor pressure over ice compared to that over liquid (Korolev, 2007; Korolev & Isaac, 2003). To consider the effect of ice formation on the supersaturation in our experiments, we adapt the approach of Korolev and Mazin (2003) to the conditions in the Π-Chamber. Specifically, we consider the competing processes for supersaturation over ice, thereby forming the differential equation

$$\frac{ds_i}{dt} = \frac{s_{i,0} - s_i}{\tau_t} - \frac{s_i}{\tau_{c,i}} - \frac{s_l}{\tau_{c,l}}. \tag{1}$$

Here s_i and s_l are the supersaturations over ice and liquid, respectively. (s_k is defined as $S_k - 1$, where $S_k \equiv e/e_k$ is the saturation ratio. e and e_k are the environmental and equilibrium vapor pressures, and k denotes either ice, i, or liquid, l.) The ice supersaturation that would be achieved in the chamber in absence of any hydrometeors is $s_{i,0}$. This is essentially determined by the imposed temperature difference, which is held constant during the experiments. Similarly, $\tau_{c,i}$ and $\tau_{c,l}$ are the phase relaxation times for ice and liquid particles, respectively, and τ_t is the turbulence mixing time. Phase relaxation time is defined as $\tau_{c,k} = (4\pi D n_k r_k)^{-1}$, where again k denotes either ice or liquid, D is the vapor diffusion constant considering latent heat release (Cooper, 1989; Rogers & Yau, 1989), and n_k and r_k are the mean particle number concentration and radius, respectively. Here we assume the shape factor for ice crystals ($c = 1$) since the ice particles in the chamber are nearly spherical due to smaller lifetimes. The first term on the right side of equation (1) indicates the relaxation of the supersaturation toward the equilibrium value (Chandrakar et al., 2016), while the second and third terms are sinks for supersaturation due to ice crystal growth and cloud droplet growth, respectively. The last term can be written in terms of ice supersaturation using $s_l = (e_i/e_l)(s_i + 1) - 1 = A(s_i + 1) - 1$ (Korolev & Mazin, 2003) . Assuming that the system is in steady state, we can solve for s_i

$$s_i = \left(\frac{s_{i,0}}{\tau_t} + \frac{1 - A}{\tau_{c,l}}\right)\left(\frac{1}{\tau_t} + \frac{1}{\tau_{c,i}} + \frac{A}{\tau_{c,l}}\right)^{-1}. \tag{2}$$

Now since this can be equated to $s_i = (s_l + 1)/A - 1$, we can solve for the condition $s_l \geq 0$, which is the condition for coexistence of liquid water and ice. After some rearranging, this results in

$$\tau_{c,i} \geq \tau_t \left(\frac{e_l - e_i}{e_0 - e_l}\right) = \tau_t \frac{s_l^\star}{s_{l,0}}, \tag{3}$$

where we have defined $s_l^\star \equiv -(e_i - e_l)/e_l$, the magnitude of the liquid-water supersaturation deficit that exists at the ice-saturation level, and denoted the liquid-water supersaturation corresponding to $s_{i,0}$ as $s_{l,0}$ (defined as the initial supersaturation in the absence of any aerosols). $s_l^\star$ is useful since measuring the exact supersaturation within the chamber in the presence of hydrometeors under supercooled conditions is difficult. It provides the supersaturation deficit for the limiting condition at $s_l \geq 0$ for existence of a mixed-phase cloud.

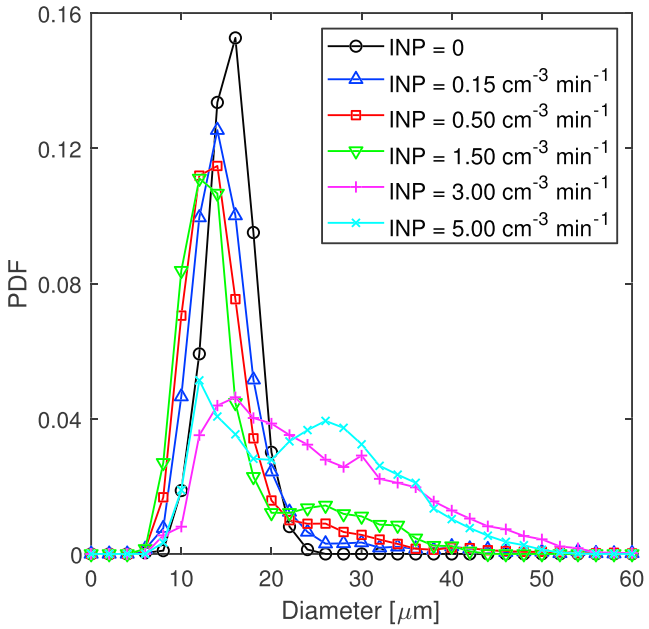

Figure 2. Probability Distribution Functions (PDF) of particle equivalent diameter are shown for various INP injection rates. As the INP injection rate increases, larger particles begin to appear, and the size distribution becomes bimodal in nature. For the purposes of this analysis, supercooled liquid droplets and ice particles are classified according to size. All particles with diameters smaller than 20 μm are considered to be water droplets, and those with larger effective diameters are considered to be ice particles. Note that the INP injection rates are shown as number per volume of air in the chamber, not as concentration in the inlet flow. INP = ice-nucleating particle.

This is consistent with prior observations of $s_{l,0}$ falling to a value close to liquid saturation once hydrometeors are generated in the chamber (Niedermeier et al., 2018). We can now write equation (3) as a condition for the ice integral radius:

$$n_i \bar{r}_i \leq \frac{1}{4\pi D \tau_t} \frac{s_{l,0}}{s_l^\star}. \quad (4)$$

The equation shows that for a given liquid-water supersaturation $s_{l,0}$, relative to the supersaturation deficit that drives the WBF process (i.e., $s_l^\star$), a critical integral radius exists at which the amount of ice leads to complete glaciation and disappearance of the liquid phase. In other words, the answer to our first motivating question is that mixed-phase clouds can be sustained as long as the product of the number and size of the ice crystals in the cloud is below a critical level, related to the cloud forcing. Equation (4) is analogous to equation 4 from Korolev (2007), where these issues are considered in the context of forcing by an updraft in a cloud, which leads to supersaturated conditions. Note that for nonspherical ice particles, an additional shape factor will be multiplied to the integral radius in equation (4), which may reduce the critical value even further. In the next section, we examine the microphysical properties of the laboratory mixed-phase cloud, further clarifying how clouds respond to the introduction of INPs.

4. Results

4.1. Size Distribution

Probability distribution functions of the measured equivalent diameter of hydrometeors for several INP injection rates are shown in Figure 2. (Henceforth, this combination of liquid droplets and ice crystals together will be referred to simply as "particles.") With no INP in the chamber (black curve), a steady-state supercooled liquid droplet distribution is observed. The mean supersaturation is close to the saturation vapor pressure over the liquid. However, with increasing INP injection rates, the size distribution begins to develop another mode close to 30 μm. This corresponds to the appearance of ice particles within the chamber and is consistent with the visual impression of "scintillating" particles illuminated in the cloud chamber (cf. center panel of Figure 1). Evidence of the WBF process can be seen in the PDFs as a continuous decrease of the mean diameter of the supercooled liquid droplets with increasing INP injection rate and corresponding increase in the ice crystal tail. This observation is consistent with the LES results of Hill et al. (2014) indicating a negative correlation between liquid water content and ice concentration in turbulent mixed-phase clouds.

The PDFs suggest that supercooled liquid is never completely eliminated, even at the highest INP injection rate, but glaciation is typically defined in terms of mass rather than number. We calculate the liquid water and ice mass fractions, assuming that all particles with a diameter greater than 20 μm are ice and that both liquid and ice are spheres (cf. Figure 1). This approach is taken because for such small particle sizes, it is challenging to distinguish liquid and ice particles based on shape alone. The 20-μm cutoff is chosen based on the large-diameter tail of the zero INP case and on the minimum between the two modes of the maximum INP case. Similar approaches have been used in other studies such as that of Niedermeier et al. (2010) where a size step classification function was used to distinguish between ice and cloud droplets. This assumption results in an ice mass fraction of 0.09 when we know that only supercooled droplets are present; we subtract that from subsequent values of ice mass fraction and the number from ice number concentration. Average ice mass fractions of 0.41, 0.56, 0.60, 0.81, and 0.82 result from the injection rates of 0.15, 0.5, 1.50, 3.00, and 5.00 cm^{-3} min^{-1}, respectively (Figure 2). The values are within the mixed-phase cloud range for measured ice fraction, with the last two close to the full-glaciation threshold of 0.9 (Korolev et al., 2003). Further examination of the behavior of averaged ice mass fraction with respect to INP injection rate is provided in Supporting Information S1.

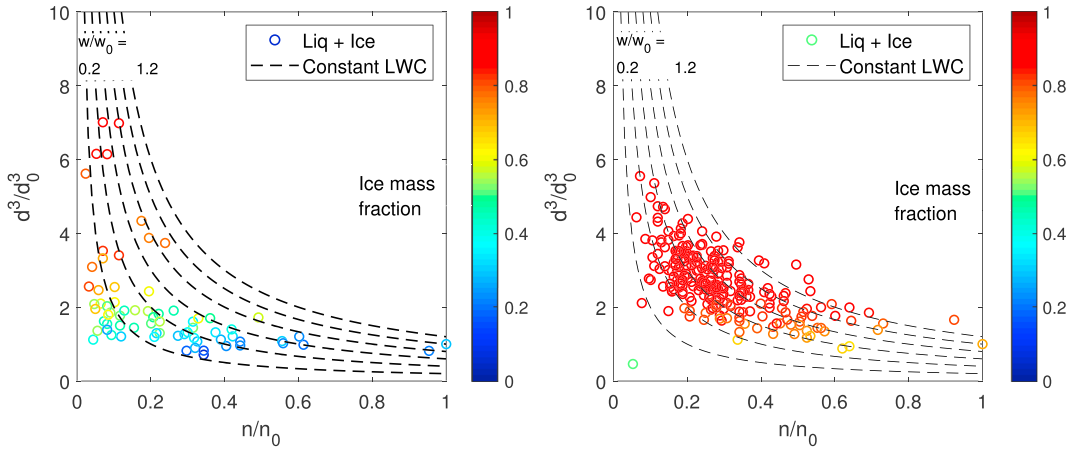

Figure 3. Mean cubed-diameter d^3 versus number concentration n of hydrometeors, with each point corresponding to a single hologram sample volume. The points are colored according to the ice mass fraction for each hologram. Contours of constant Liquid Water Content (LWC) ($w \propto nd^3$) are shown as dashed lines. Measurements are from experiments with ice-nucleating particle injection rates of 0.15 cm^{-3} min^{-1} (left) and 5.00 cm^{-3} min^{-1} (right). All values are normalized by the n_0 and d_0^3 from the hologram containing maximum water content w_0.

Another perspective on mixed-phase conditions results by considering how liquid water and ice are partitioned within the cloud, that is, to what extent are they well mixed? Figure 3 shows the ice mass fractions within individual hologram sample volumes for INP injection rates of 0.15 cm^{-3} min^{-1} (left panel) and 5.00 cm^{-3} min^{-1} (right panel). The results are shown in a (n, d^3) space, and points are observed to roughly lie along constant water content contours. Especially in the low-ice-content case (left panel), it is observed that ice and liquid water are strongly partitioned, with ice appearing in small numbers and large particle sizes and cloud droplets appearing in relatively high concentrations and small diameters. Finally, the right panel further confirms that the cloud is nearly fully glaciated at the highest INP injection rate.

4.2. INP-Activated Fraction and Cloud Glaciation

We now proceed to check for consistency between the observations and the theoretical threshold for glaciation given by equation (4). To calculate the INP injection rate that leads to complete glaciation of the cloud, we first determine the relation between INP input and observed ice crystal concentration. Specifically, we can test whether it is reasonable to assume that all of the injected INP nucleate ice, as would be suggested for the temperature of these experiments (Wex et al., 2015). With the source known, we need a removal rate to determine the concentration in the chamber. In steady state, the input of INP is balanced by the removal of ice crystals through sedimentation, where that removal rate is equal to the ice concentration divided by the particle residence time inside the cloud:

$$\frac{\mathrm{d}n_\mathrm{i}}{\mathrm{d}t}\Big|_{\mathrm{injected}} = \frac{n_\mathrm{i}}{\tau_\mathrm{res}}. \tag{5}$$

Since most of the ice particles are close to spherical, we can approximate τ_res of a particle having mean radius, $\bar{r}$, and falling over the height of the chamber $H = 1$ m (Yang et al., 2013)

$$\tau_\mathrm{res} = \left(\frac{H}{k\xi\overline{s_\mathrm{i}}}\right)^{1/2}, \tag{6}$$

where $\bar{s}$ is the mean supersaturation experienced by the particle as it falls, $k = 1.2\times10^8$ m^{-1} s^{-1} is the Stokes coefficient, and ξ is the thermodynamic growth parameter. If the conditions are saturated with respect to water, $\overline{s_\mathrm{i}}$ experienced by the particle is approximately 6.9% (Rogers & Yau, 1989) for a mean temperature of −6.7 °C. This gives us a residence time of $\tau_\mathrm{res} = 52.8$ s. The corresponding expected ice particle concentration is shown in the left panel of Figure 4. The predicted (blue circles) and measured (red squares) ice concentrations agree to within the experimental uncertainty. The black line in both panels of Figure 4 is the apparent background ice concentration, derived from measurements when no INP were being injected. The nonzero value is due to the fact that we have classified everything with a diameter greater than 20 μm as ice, when in fact, there are a few liquid water droplets of that size, especially for the low INP injection cases.

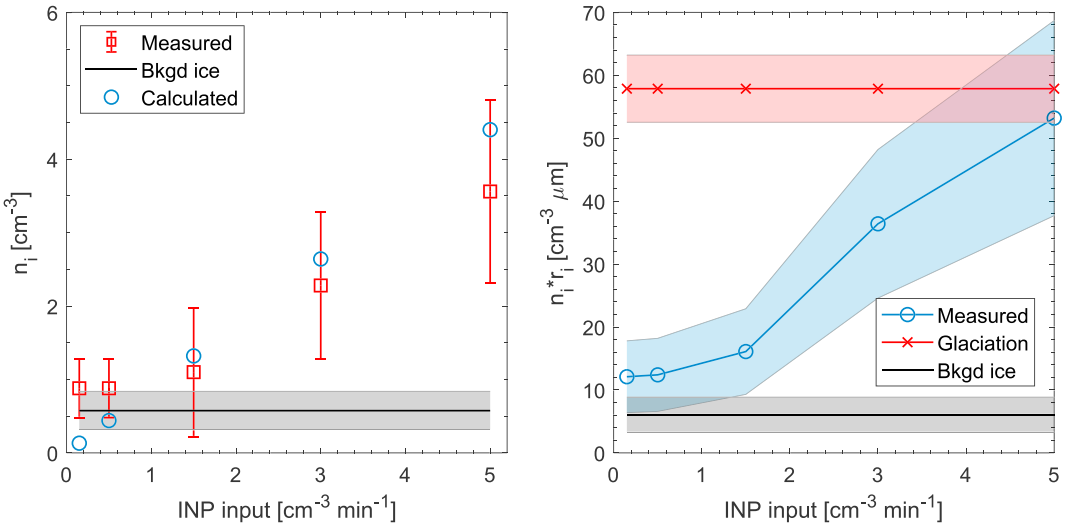

Figure 4. (left) The calculated ice number concentration (blue circle) is compared with the measured ice number concentration (red square) as a function of INP injection rate. The error bars correspond to the standard deviation in the measured mean concentration. This shows that the measured values of ice number concentration are close to but less than those expected for a 100% conversion of INP to ice. (right) Ice integral radius required for glaciation of mixed-phase cloud is shown in red, while measured values of ice integral radius are shown in blue. This shows that for a sufficiently high INP input rate, one can achieve glaciation of a mixed-phase cloud. INP = ice-nucleating particle.

Equations (3) and (4) are expressions for a bound on the ice phase relaxation time or integral radius required to sustain coexistence of ice and supercooled liquid water, that is, mixed-phase conditions. We measure the size and concentration of ice in the experiments, so we can compare the measurements to the prediction, if we know the required supersaturation $s_{l,0}$. However, measuring supersaturation is quite challenging; to circumvent this, we, instead, use the stochastic condensation approach outlined in Desai et al. (2018). The method requires an estimate of the turbulence mixing time, τ_t, for the Π-chamber, which we obtain from measurements of the time required by the chamber to relax back to an equilibrium condition after a perturbation. That results in $\tau_t = 61.2$ s and $s_l = 0.01$, which then leads to an inferred initial supersaturation of $s_{l,0} = 0.031$. In other words, the liquid-water supersaturation in the chamber when no CCN or INP are present is 3.1%.

With estimates of $s_{l,0}$ and $s_l^\star$, we can compute the predicted value for the ice integral radius required for complete glaciation of the cloud. Figure 4 shows this value in red, along with its uncertainty (red shading). The ice integral radii, derived from the measurements, are shown in blue, again with shading for the uncertainty. We see that for the INP injection rates in our experiment, we are just able to approach glaciation, which is consistent with the ice mass fractions estimated above. Although the expression we are using for the theory is in a somewhat different form, we take this as direct experimental validation of the analogous expression derived in Korolev and Isaac (2003).

5. Discussion

The experiments reported here yield at least three significant findings. First, steady-state mixed-phase clouds can be generated through a balance of fluxes, between supersaturation forcing, nucleation, and growth rate of ice crystals and ice crystal precipitation. Even in these steady conditions, ice and liquid water tend to be segregated from each other. Second, the Korolev-Mazin approach that identifies the ice integral radius or ice phase relaxation time as the critical thresholds for glaciation is consistent with the observations. Third, for fixed forcing, the ice to total water content is controlled by the number of INPs (under the implicit assumption that CCN are plentiful). These findings benefit from the ability to perform relatively simplified experiments in the Π-Chamber: The only processes considered are cloud droplet activation, ice nucleation, growth of droplets/ice by condensation/deposition, and particle sedimentation. Other complicating factors that often are present in natural clouds, such as riming, coalescence, and aggregation, are not present. Most

significantly, the thermodynamic forcing is fixed, so that confounding effects of feedbacks between the cloud microphysics and the cloud dynamics are eliminated.

The theory and measurements shown in the preceding two sections are a different perspective on the WBF process occurring in clouds, which is most commonly associated with growth of ice crystals at the expense of liquid droplets (Korolev & Isaac, 2003); that is, cloud glaciation occurs as supercooled cloud droplets are evaporated. However, that is true for a transition from a supercooled liquid cloud with a few ice particles to a completely glaciated one. The perspective for a steady-state mixed-phase cloud requires a slightly different interpretation. The larger the concentration of ice particles in a steady-state cloud, the lower the mean supersaturation will be within the range defined by the difference in the saturation vapor pressure between ice particles and water droplets. This is consistent with LES studies, such as that of Hill et al. (2014), showing that as ice number concentration increases, cloud droplet activation is more strongly inhibited. Hence, for a critical ice number concentration and size, the mean supersaturation of the cloud parcel can be reduced to a value that will prevent any new CCN from activating and thereby lead to an ice only cloud without evaporation of cloud droplets (equation (4)).

In the atmosphere, achieving glaciation through a large INP concentration is likely rare, given typical concentrations of 0.01 to 100 L^{-1} (Rogers & Yau, 1989, p. 244). However, as equation (4) and our measurements show, it is not number alone that determines whether a cloud will convert to ice. Rather, it is the sink of water vapor that the ice provides, which is controlled by its integral radius. While the number concentration of ice particles in the Π Chamber is much higher than that found in typical atmospheric clouds, the ice integral radius is within the range found in the atmosphere, $0.5 < n_i r_i < 500$ μm/cm^3 (Korolev, 2008). (The 1-m height of the chamber limits the lifetime of crystals larger than ∼50-μm diameter; we achieve larger integral radii by increasing the number of injected INP.) Note that while equation (4) is the condition for ice-liquid coexistence in the chamber, the time scale to approach glaciation, for example, is $\tau_{sys} = \left(\frac{1}{\tau_t} + \frac{1}{\tau_i} + \frac{A}{\tau_l}\right)^{-1}$ (Korolev & Mazin, 2003), which for our highest INP injection rates is ≃45 s. (See Supporting Information S1 for distributions of the liquid and ice phase relaxation times.) Higher injection rates (and thus higher values of $n_i r_i$) would result in glaciation on shorter time scales. In atmospheric clouds, certain extreme scenarios may give rise to such concentrations (Hobbs et al., 1981; Stith et al., 1978). The effect of such high INP concentrations is similar to the cloud "overseeding" concept explored by Mason, (1971, p.369) and Durant et al. (2008), which could lead to a reduction in particle size and collapse of the WBF process (Rokicki & Young, 1978; Young, 1993).

The WBF process continues to be a source of unforeseen intricacies, and the results presented here illuminate yet another facet. The core idea originally expressed by Wegener in 1911 was "The consequence must then be that continuous condensation takes place on the ice while at the same time liquid water evaporates continually, and this process must persist until the liquid phase is completely consumed." Thus, from the beginning, the notion of transience was instilled. Over time, it has become apparent that the process need not necessarily be transient because it can be driven by radiative cooling or other forcing mechanisms balanced by ice crystal removal through sedimentation (e.g., Fridlind et al., 2012; Yang et al., 2013), although even in those modeling studies, the idealized steady state is never strictly achieved. Implementation of the WBF process in weather and climate models has been challenging and rests on assumptions about how liquid water and ice are partitioned, how they interact diffusively, and so on (Baumgartner & Spichtinger, 2018; Castellano et al., 2004; Storelvmo et al., 2008). Understanding of aerosol indirect effects involving mixed-phase clouds is even more uncertain, but there is ample field evidence for a strong role of aerosols (Fan et al., 2017; Jouan et al., 2012; Prenni et al., 2007; Vergara-Temprado et al., 2018). The perspectives brought into focus through these laboratory experiments will help in understanding the interplay between supersaturation forcing and ice nucleation and the implications for aerosol-mediated cloud glaciation.

Acknowledgments
This work was supported by National Science Foundation Grant AGS-1754244 and by NASA Headquarters under the NASA Earth and Space Science Fellowship Program Grant 80NSSC17K0449. Portage, a high-performance computing infrastructure at Michigan Technological University, was used in obtaining results presented in this publication. Data used in this study are available online (https://digitalcommons.mtu.edu/physics-fp/302/).

References

Baumgartner, M., & Spichtinger, P. (2018). Towards a bulk approach to local interactions of hydrometeors. *Atmospheric Chemistry and Physics*, *18*(4), 2525–2546.

Castellano, N. E., Avila, E. E., & Saunders, C. P. (2004). Theoretical model of the Bergeron–Findeisen mechanism of ice crystal growth in clouds. *Atmospheric Environment*, *38*(39), 6751–6761.

Chandrakar, K. K., Cantrell, W., Chang, K., Ciochetto, D., Niedermeier, D., Ovchinnikov, M., et al. (2016). Aerosol indirect effect from turbulence-induced broadening of cloud-droplet size distributions. *Proceedings of the National Academy of Sciences of the United States of America*, *113*, 14,243–14,248.

Chang, K., Bench, J., Brege, M., Cantrell, W., Chandrakar, K., Ciochetto, D., et al. (2016). A laboratory facility to study gas-aerosol-cloud interactions in a turbulent environment: The π chamber. *Bulletin of the American Meteorological Society*, *97*, 2343–2358.
Cooper, W. A. (1989). Effects of variable droplet growth histories on droplet size distributions. Part I: Theory. *Journal of the Atmospheric Sciences*, *46*, 1301–1311.
Curry, J., Pinto, J., Benner, T., & Tschudi, M. (1997). Evolution of the cloudy boundary layer during the autumnal freezing of the Beaufort Sea. *Journal of Geophysical Research*, *102*(D12), 13,851–13,860.
Desai, N., Chandrakar, K., Chang, K., Cantrell, W., & Shaw, R. (2018). Influence of microphysical variability on stochastic condensation in a turbulent laboratory cloud. *Journal of the Atmospheric Sciences*, *75*(1), 189–201.
Durant, A. J., Shaw, R., Rose, W. I., Mi, Y, & Ernst, G. (2008). Ice nucleation and overseeding of ice in volcanic clouds. *Journal of Geophysical Research*, *113*, D09206. https://doi.org/10.1029/2007JD009064
Fan, J., Leung, L. R., Rosenfeld, D., & DeMott, P. J. (2017). Effects of cloud condensation nuclei and ice nucleating particles on precipitation processes and supercooled liquid in mixed-phase orographic clouds. *Atmospheric Chemistry and Physics*, *17*(2), 1017–1035.
Field, P., & Heymsfield, A. (2015). Importance of snow to global precipitation. *Geophysical Research Letters*, *42*, 9512–9520. https://doi.org/10.1002/2015GL065497
Fridlind, A. M., Van Diedenhoven, B., Ackerman, A. S., Avramov, A., Mrowiec, A., Morrison, H., et al. (2012). A FIRE-ACE/SHEBA case study of mixed-phase arctic boundary layer clouds: Entrainment rate limitations on rapid primary ice nucleation processes. *Journal of the Atmospheric Sciences*, *69*(1), 365–389.
Fu, S., & Xue, H. (2017). The effect of ice nuclei efficiency on Arctic mixed-phase clouds from large-eddy simulations. *Journal of the Atmospheric Sciences*, *74*(12), 3901–3913.
Fugal, J. P., Shaw, R. A., Saw, E. W., & Sergeyev, A. V. (2004). Airborne digital holographic system for cloud particle measurements. *Applied Optics*, *43*, 5987–5995.
Furtado, K, Field, P., Boutle, I., Morcrette, C., & Wilkinson, J. (2016). A physically based subgrid parameterization for the production and maintenance of mixed-phase clouds in a general circulation model. *Journal of the Atmospheric Sciences*, *73*, 279–291.
Garrett, T. J., & Zhao, C. (2006). Increased Arctic cloud longwave emissivity associated with pollution from mid-latitudes. *Nature*, *440*(7085), 787–789.
Hill, A., Field, P., Furtado, K, Korolev, A, & Shipway, B. (2014). Mixed-phase clouds in a turbulent environment. Part 1: Large-eddy simulation experiments. *Quarterly Journal of the Royal Meteorological Society*, *140*(680), 855–869.
Hobbs, P. V., Radke, L. F., Eltgroth, M. W., & Hegg, D. A. (1981). Airborne studies of the emissions from the volcanic eruptions of Mount St. Helens. *Science*, *211*(4484), 816–818.
Jouan, C., Girard, E., Pelon, J., Gultepe, I., Delanoë, J., & Blanchet, J.-P. (2012). Characterization of Arctic ice cloud properties observed during ISDAC. *Journal of Geophysical Research*, *117*, D23207. https://doi.org/10.1029/2012JD017889
Kalesse, H., de Boer, G., Solomon, A., Oue, M., Ahlgrimm, M., Zhang, D., et al. (2016). Understanding rapid changes in phase partitioning between cloud liquid and ice in stratiform mixed-phase clouds: An Arctic case study. *Monthly Weather Review*, *144*(12), 4805–4826.
Kay, J. E., & Gettelman, A. (2009). Cloud influence on and response to seasonal Arctic sea ice loss. *Journal of Geophysical Research*, *114*, D18204. https://doi.org/10.1029/2009JD011773
Korolev, A. (2007). Limitations of the Wegener–Bergeron–Findeisen mechanism in the evolution of mixed-phase clouds. *Journal of the Atmospheric Sciences*, *64*(9), 3372–3375.
Korolev, A. (2008). Rates of phase transformations in mixed-phase clouds. *Quarterly Journal of the Royal Meteorological Society*, *134*(632), 595–608.
Korolev, A., & Isaac, G. (2003). Phase transformation of mixed-phase clouds. *Quarterly Journal of the Royal Meteorological Society*, *129*(587), 19–38.
Korolev, A., Isaac, G. A., Cober, S. G., Strapp, W. J., & Hallett, J. (2003). Microphysical characterization of mixed-phase clouds. *Quarterly Journal of the Royal Meteorological Society*, *129*(587), 39–65.
Korolev, A., & Mazin, I. P. (2003). Supersaturation of water vapor in clouds. *Journal of the Atmospheric Sciences*, *60*(24), 2957–2974.
Korolev, A., McFarquhar, G., Field, P. R., Franklin, C., Lawson, P., Wang, Z., et al. (2017). Mixed-phase clouds: Progress and challenges. *Meteorological Monographs*, *58*, 5.1–5.50.
Lamb, D., & Verlinde, J. (2011). *Physics and chemistry of clouds*. Cambridge: Cambridge University Press.
Lawson, R. P., Woods, S., & Morrison, H. (2015). The microphysics of ice and precipitation development in tropical cumulus clouds. *Journal of the Atmospheric Sciences*, *72*(6), 2429–2445.
Lohmann, U. (2002). A glaciation indirect aerosol effect caused by soot aerosols. *Geophysical Research Letters*, *29*(4), 1052. https://doi.org/10.1029/2001GL014357
Lu, J., Fugal, J. P., Nordsiek, H., Saw, E. W., Shaw, R. A., & Yang, W. (2008). Lagrangian particle tracking in three dimensions via single-camera in-line digital holography. *New Journal of Physics*, *10*, 125013.
Mülmenstädt, J., Sourdeval, O., Delanoë, J., & Quaas, J. (2015). Frequency of occurrence of rain from liquid-, mixed-, and ice-phase clouds derived from A-Train satellite retrievals. *Geophysical Research Letters*, *42*, 6502–6509. https://doi.org/10.1002/2015GL064604
Mason, B. (1971). *The physics of clouds*. Oxford: Clarendon Press.
McFarquhar, G. M., & Cober, S. G. (2004). Single-scattering properties of mixed-phase Arctic clouds at solar wavelengths: Impacts on radiative transfer. *Journal of Climate*, *17*(19), 3799–3813.
Morrison, H., De Boer, G., Feingold, G., Harrington, J., Shupe, M. D., & Sulia, K. (2012). Resilience of persistent Arctic mixed-phase clouds. *Nature Geoscience*, *5*(1), 11–17.
Niedermeier, D., Chang, K., Cantrell, W., Chandrakar, K. K., Ciochetto, D., & Shaw, R. A. (2018). Observation of a link between energy dissipation rate and oscillation frequency of the large-scale circulation in dry and moist Rayleigh-Bénard turbulence. *Physical Review Fluids*, *3*(8), 83501.
Niedermeier, D., Hartmann, S., Shaw, R., Covert, D., Mentel, T., & Schneider, J. (2010). Heterogeneous freezing of droplets with immersed mineral dust particles—Measurements and parameterization. *Atmospheric Chemistry and Physics*, *10*, 3601–3614.
Norgren, M. S., Boer, G. d., & Shupe, M. D. (2018). Observed aerosol suppression of cloud ice in low-level Arctic mixed-phase clouds. *Atmospheric Chemistry and Physics*, *18*(18), 13,345–13,361.
Pinsky, M., Khain, A., & Korolev, A. (2018). Theoretical analysis of liquid–ice interaction in the unsaturated environment with application to the problem of homogeneous mixing. *Journal of the Atmospheric Sciences*, *75*(4), 1045–1062.
Pinto, J. O. (1998). Autumnal mixed-phase cloudy boundary layers in the Arctic. *Journal of the Atmospheric Sciences*, *55*(11), 2016–2038.
Prenni, A. J., Harrington, J. Y., Tjernström, M., DeMott, P. J., Avramov, A., Long, C. N., et al. (2007). Can ice-nucleating aerosols affect Arctic seasonal climate? *Bulletin of the American Meteorological Society*, *88*(4), 541–550.
Rogers, R., & Yau, M. (1989). *A short course in cloud physics*. Oxford: Butterworth-Heinemann.

Rokicki, M. L., & Young, K. C. (1978). The initiation of precipitation in updrafts. *Journal of Applied Meteorology and Climatology*, *17*(6), 745–754.

Shupe, M. D., Matrosov, S. Y., & Uttal, T. (2006). Arctic mixed-phase cloud properties derived from surface-based sensors at SHEBA. *Journal of the Atmospheric Sciences*, *63*(2), 697–711.

Shupe, M. D., Walden, V. P., Eloranta, E., Uttal, T., Campbell, J. R., Starkweather, S. M., & Shiobara, M. (2011). Clouds at Arctic atmospheric observatories. Part I: Occurrence and macrophysical properties. *Journal of Applied Meteorology and Climatology*, *50*(3), 626–644.

Stith, J. L., Hobbs, P. V., & Radke, L. F. (1978). Airborne particle and gas measurements in the emissions from six volcanoes. *Journal of Geophysical Research*, *83*(C8), 4009–4017.

Storelvmo, T, Kristjánsson, J., Lohmann, U, Iversen, T, Kirkevåg, A, & Seland, Ø (2008). Modeling of the Wegener–Bergeron–Findeisen process—Implications for aerosol indirect effects. *Environmental Research Letters*, *3*(4), 45001.

Sun, Z., & Shine, K. P. (1995). Parameterization of ice cloud radiative properties and its application to the potential climatic importance of mixed-phase clouds. *Journal of Climate*, *8*(7), 1874–1888.

Vergara-Temprado, J., Miltenberger, A. K., Furtado, K., Grosvenor, D. P., Shipway, B. J., Hill, A. A., et al. (2018). Strong control of Southern Ocean cloud reflectivity by ice-nucleating particles. *Proceedings of the National Academy of Sciences of the United States of America*, *115*(11), 2687–2692.

Verlinde, J., Harrington, J. Y., McFarquhar, G., Yannuzzi, V., Avramov, A., Greenberg, S., et al. (2007). The mixed-phase Arctic cloud experiment. *Bulletin of the American Meteorological Society*, *88*(2), 205–222.

Westbrook, C., & Illingworth, A. (2013). The formation of ice in a long-lived supercooled layer cloud. *Quarterly Journal of the Royal Meteorological Society*, *139*(677), 2209–2221.

Wex, H., Augustin-Bauditz, S., Boose, Y., Budke, C., Curtius, J., Diehl, K., et al. (2015). Intercomparing different devices for the investigation of ice nucleating particles using Snomax® as test substance. *Atmospheric Chemistry and Physics*, *15*(3), 1463–1485.

Yang, F., Ovchinnikov, M., & Shaw, R. A. (2013). Minimalist model of ice microphysics in mixed-phase stratiform clouds. *Geophysical Research Letters*, *40*, 3756–3760. https://doi.org/10.1002/grl.50700

Young, K. C. (1993). *Microphysical processes in clouds*. Oxford: Oxford Univ. Press.

Zawadzki, I, Szyrmer, W, & Laroche, S (2000). Diagnostic of supercooled clouds from single-doppler observations in regions of radar-detectable snow. *Journal of Applied Meteorology and Climatology*, *39*(7), 1041–1058.